Symposium Article

Evolution of silk anchor structure as the joint effect of spinning behavior and spinneret morphology

Running head: Evolution of spider silk anchor assembly

Jonas O. Wolff[1*], Peter Michalik[2], Alexandra M. Ravelo[3], Mariella E. Herberstein[1], and Martín J. Ramírez[3]

[1] Department of Biological Sciences, Macquarie University, Sydney, NSW 2109, Australia

[2] Zoologisches Institut und Museum, Ernst-Moritz-Arndt-Universität, Loitzer Str. 26, 17489, Greifswald, Germany

[3] Museo Argentino de Ciencias Naturales "Bernardino Rivadavia", Consejo Nacional de Investigaciones Científicas y Técnicas (CONICET), Av. Ángel Gallardo 470, C1405DJR, Buenos Aires, Argentina

* corresponding author: jonas.wolff@mq.edu.au

Word count: 5877

Abstract

Spider web anchors are attachment structures composed of the bi-phasic glue-fiber secretion from the piriform silk glands. The mechanical performance of the anchors strongly correlates with the structural assembly of the silk lines, which makes spider silk anchors an ideal system to study the biomechanical function of extended phenotypes and its evolution. It was proposed that silk anchor function guided the evolution of spider web architectures, but its fine-structural variation and whether its evolution was rather determined by changes of the shape of the spinneret tip or in the innate spinning choreography remained unresolved. Here, we comparatively studied the micro-structure of silk anchors across the spider tree of life, and set it in relation to spinneret morphology, spinning behavior and the ecology of the spider. We identified a number of apomorphies in the structure of silk anchors that may positively affect anchor function: 1. bundled dragline, 2. dragline envelope, and 3. dragline suspension ('bridge'). All these characters were apomorphic and evolved repeatedly in multiple lineages, supporting the notion that they are adaptive. The occurrence of these structural features can be explained with changes in the shape and mobility of the spinneret tip, the spinning behavior or both. Spinneret shapes generally varied less than their fine-tuned movements, indicating that changes in construction behavior play a more important role in the evolution of silk anchor assembly. However, the morphology of the spinning apparatus is also a major constraint to the evolution of the spinning choreography. These results highlight changes in behavior as the proximate and in morphology as the ultimate causes of extended phenotype evolution. Further, this research provides a roadmap for future bioprospecting research to design high-performance instant line anchors.

Keywords

spider silk, spider web, bioadhesion, attachment disc, anterior lateral spinneret, piriform silk

1. Introduction

Spiders are one of the most successful and dominant groups of invertebrate predators in terrestrial ecosystems (Foelix 2011; Nyffeler and Birkhofer 2017). This success is largely attributed to the evolution of a unique material – spider silk. Spider silk is assembled into functional structures such as webs and cocoons. The architecture and function of such products is often clade-specific – they can be regarded as phenotypic gene expressions outside of the body, so-called extended phenotypes (Dawkins 1982). Several factors play a role in the generation of extended phenotype morphologies and functions, including *environmental* factors, such as the substrate upon which the architecture is built or the properties of environmental materials used in construction, and *organismal* factors, such as sequences of building behavior, the organs used in construction and the properties of secreted building materials. The differences in significance and interplay between these factors in the evolution of extended phenotype function is poorly understood.

Spider silk anchors (also called *attachment discs*) are small depositions of the two-phasic glue-fiber secretions of the piriform silk glands (Kovoor and Zylberberg 1980; Wirth et al. 2019) used to attach silk lines to environmental substrates or to other silk lines (Fig. 1). Consequently, silk anchors are highly important for the assembly of silk lines into complex architectures. Thereby, each anchor is a fiber assembly in its own regard, composed of numerous piriform silk nanofibers that are arranged in a specific way around the structural silk line (the latter of which is mainly composed of the secretions of the ampullate silk glands) (Wolff et al. 2015; Wolff and Herberstein 2017). Both empirical and numerical studies have demonstrated that with the same type of building material differences in the anchor's attachment strength can be produced by differences in its behavioral assembly (Sahni et al. 2012; Pugno et al. 2013; Wolff et al. 2017b; 2019). This highlights construction behavior as an important determinant of anchor function.

Anchor structure varies between species and is dependent on evolutionary history (Wolff et al. 2017b; 2019). Experiments have shown that anchor structure is barely affected by the environment (Wolff et al. 2020) nor by the body condition of the spider (Wolff et al. 2018). Thus, spider silk anchors represent an ideal system to disentangle the effects of the morphology of the organs involved in construction (the anterior lateral spinnerets) and the construction behavior (spinneret kinematics) on the structure and function of the extended phenotype (the silk anchor).

We previously found that anchor geometry affects the attachment strength of the anchor and correlates with the innate spinning choreography of the anterior lateral spinnerets that bear

the piriform and major ampullate gland spigots (Wolff et al. 2017b; 2019). The evolutionary enhancement of silk anchor performance was a repeated and stepwise event and was linked to the evolution of aerial webs (Wolff et al. 2019) – a key innovation in spider evolution that opened the niche of preying upon flying insects. However, differences in the structure of the dragline joint and the generation thereof, remained unclear. This is significant, because the way the dragline is connected to the piriform silk film can affect how tensile stress is transmitted onto the silk-substrate adhesive interface. For instance, in orb web spiders, the dragline fibers are bundled within a piriform silk envelope that is suspended in a network of radially arranged piriform silk fibers ('*bridge*' sensu Grawe et al. 2014), which may explain the enhanced insensitivity towards varying loading angles observed in the anchors of these spiders (Wolff and Herberstein 2017; Wolff et al. 2017b).

Here, we studied the microstructure of silk anchors across the spider tree of life to describe the distribution of distinct anchor architectures. This was combined with an analysis of spinneret morphology and spinning behavior to unravel their relative effects on anchor structure. To clarify if differences in anchor architecture are adaptations towards different functions their macro-evolutionary trends were studied in a phylogenetic comparative framework and set in relationship with foraging ecology.

2. Material and Methods

2.1. Animals. Spiders were collected in Australia (New South Wales, Queensland and Tasmania), New Zealand (North and South Island) and Germany, with some additions of material from Italy, Czechia, Morocco, Thailand and the U.S.A., or sourced from lab stocks (4 species). Fieldwork in Australia was performed under licenses SL101868, FA 18285 and PTU19-001938, and in New Zealand under licenses 64293-RES and 71225-RES. In total, individuals of 204 species from 62 families were observed, including all major evolutionary lineages of the araneomorph tree of life. In addition, two mygalomorph species (from two families) were observed as an outgroup sample. For the full species list, the origins, sample sizes and voucher deposition, see S1.

The majority of silk samples were obtained by placing microscopy glass slides into the spider's container, which were removed after spiders had deposited silk on them. In a few cases samples were obtained by letting the spider walk underneath the glass slide, which usually triggered silk anchoring behavior. For *Argyroneta aquatica* this was done in a water filled petri dish.

2.2. Microscopy. Silk anchors on glass slides were imaged with Leica M205A (Leica Microsystems GmbH, Wetzlar, Germany) and Motic (Motic Inc. Ltd., Hong Kong) stereo microscopes, or an Olympus BH-2 (Olympus Co., Tokyo, Japan) compound microscope, with mounted cameras. Samples were illuminated with diffuse reflected light or phase contrast transmission light to visualize the fibers. To facilitate the recognition of different fibers in the microscopy images used in figures, these were edited in ImageJ (Schneider et al. 2012) as follows: rescaling, adjustment of brightness and contrast, and sharpening.

For scanning electron microscopy, silk samples were collected on metal stubs, air dried and sputter coated with gold-palladium. Samples were viewed in a FEI-XL30TMP SEM (Thermo Fisher Scientific, Waltham, MA, USA), under high vacuum. Additional samples were prepared from fractioned silk anchors to gain information on the material properties and internal structure of the piriform silk (i.e. by pulling off anchors spun on glass or plastic substrates or by tearing apart anchors that were delaminated from plastic surfaces). These samples were sputter coated with chromium, which produces smaller grain sizes than gold or palladium and therefore permits a better visualization of nanostructures. Samples were observed in a JEOL JSM 7100F FESEM (JEOL, Ltd., Tokyo, Japan).

2.3. Micro-computed tomography (μCT). Specimens for μCT were either prepared from (<1 year old) ethanol material (stored in 70-80% EtOH) or freshly prepared from living spiders. In the latter case the opisthosoma was separated from the spider and fixed in Dubosq-Brazil solution. The specimens were dehydrated in graded ethanol and then critical point dried and mounted onto plastic sticks. Specimens were scanned with an Xradia MicroXCT-200 X-ray imaging system (Carl Zeiss X-ray Microscopy, Pleasanton, CA, USA). Tomography projections were reconstructed using XM Reconstructor (Carl Zeiss X-ray Microscopy, Pleasanton, CA, USA) and resulting image stacks were processed (i.e., volume renderings) with Amira 6 (Thermo Fisher Scientific, Waltham, MA, USA).

2.4. Spinneret kinematics. Spinneret movements were filmed from underneath a glass slide onto which the spider was spinning the anchor, using a Basler Ace 640×480pix USB 3.0 high speed video camera. The methodology is described in detail in Wolff and Herberstein (2017) and Wolff (2020). The position of spigot fields of active spinnerets was tracked with the *MTrackJ* plugin (Meijering et al. 2012) in *ImageJ* 1.5 (Schneider et al. 2012), as described in detail in Wolff and Herberstein (2017) and Wolff (2021).

2.5. Phylogenetic comparative framework. For the comparative analysis the phylogeny was taken from Wolff (2020). The following characters were determined from microscopy images and binary coded: (1) dragline parallel (i.e. dragline fibers run straight through the anchor in parallel to each other and do not follow the loops of the piriform silk fibers); (2) dragline envelope (i.e. the dragline fibers are bundled and clearly enclosed in a more or less cylindrical whitish mass of piriform silk; (3) bridge (i.e. the dragline is, at least in part, suspended above the plaque in a network of unattached piriform silk fiber bundles). Character evolution was modelled by stochastic character mapping with 100 iterations in *phytools* (Revell 2012), using Equal Rates (ER) or All Rates Different (ARD) substitution models. These models assume that rates of character gains and losses occur either at same rates (ER) or at asymmetric rates (ARD). The model fit was determined by calculating the corrected Akaike Information Criterion weights (AICcW).

3. Results and Discussion

3.1. Description of silk anchor structure and spinning behavior

3.1.1. General anchor structure

Occurrence of silk anchors. Silk line anchors were only observed in araneomorph spiders. Mygalomorphs were found to attach silk fibers directly to substrate and spin sheets instead of lines (Fig. S2.1a,b; also see Eberhard & Hazzi 2013 and Wolff & Gorb 2016).

General structure. Silk anchors were generally more or less bilateral-symmetric with the central symmetry line representing the dragline laying direction (equivalent with the body axis of the spider). The anchor architecture comprised a thin film of regularly arranged piriform fibers attached to the substrate (the *plaque*) and the non-adhesive *dragline*, which exits the anchor at some point. The shape of the plaque and the arrangement and density of piriform fibers differed between species and often mirrored the innate movement patterns performed with the spinnerets during anchor production (see details further below).

Types of dragline joints. We observed distinct types of dragline joints, which were considered important for the mechanical coupling and stress distribution between dragline and plaque. The dragline was either (a) directly embedded into the plaque, (b) enclosed in a tubular piriform silk envelope (*dragline envelope*) attached to the middle part of the plaque, or (c) suspended above the plaque by a network of piriform fibers not directly in contact with the substrate (*bridge*, Figs. 2A,B, 3). The bridge was often, but not always, combined with a

dragline envelope. If the dragline was directly embedded in the plaque the dragline fibers could either more or less follow the looped patterns of the piriform silk fibers in the plaque (in this case, they were not bundled nor running in parallel) or run in parallel along the central symmetry axis of the plaque. If a dragline envelope was present the dragline usually left the plaque (and the envelope) as a bundled thread, whereas dragline fibers usually left the plaque separately, if no envelope or bridge was present.

Types of dragline anchors. Spiders usually produced two types of dragline anchors: (1) *continuous* dragline anchors, i.e. an anchor spun to attach an existing dragline, in which there was an entering (*downstream*) and a leaving (*upstream*) part, or (2) *discontinuous* dragline anchors, i.e. anchors that started a dragline, in which case there was only an upstream (exiting) part and dragline initiation was represented by a whitish silk globule at the opposite end of the anchor. Discontinuous dragline anchors were more often observed in cursorial spiders than in web builders. This may be explained with the rapid and sudden locomotion of many species of cursorial spiders (where a dragline may be hindering) and their equipment with adhesive foot pads that may reduce the need for safety lines (Wolff and Gorb 2015).

Directionality. In its function as a safety line during locomotion, the main load acting on the dragline is at the end that faces the spider (i.e., the upstream end). The point where the upstream dragline connects with the anchor is called *'loading point'*. The loading point was often reinforced, e.g. by an extended silk bridge, which may give the anchor a directionality (see Fig. 2A, and in-depth description in Wolff & Herberstein 2017). Directionality may also be given by asymmetric spinneret motion patterns (i.e. stronger abductions into the anterio-lateral than the posterio-lateral direction) or a gradual increase of spinneret abductions towards the end of the spinning sequence (as often observed in araneoids). Interestingly, a previous study has proposed that anchor directionality may be used as a tactile cue by conspecifics following draglines to indicate in which direction a potential mating partner was moving (Diikstra 1976).

Construction material. We performed fracture tests of anchors from a number of species, which provided some information on the nanostructure and mechanical behavior of the piriform silk, the anchors are built of (Fig. 2). In agreement with previous fractographic (Wolff et al. 2017a) and transmission electron microscopy studies (Wirth et al. 2019), we found that the piriform silk of anchors was generally composed of an elastic central fiber that exhibited an irregular nano-fibrillar fracture face, and a glue coat with an isotropic skin and a nano-fibrillar core (Figs. 2C-K). Difference in fracture face morphology suggests differences in composition and mechanical properties. Nevertheless, the adhesion between the fiber and

the glue phases appeared strong as they were rarely separated in the fracture faces. The glue was spread out into a very thin film on the substrate (e.g. Fig. 2K). Regularly spaced cracks in the glue skin of stressed fibers and their absence over the core fiber indicated a higher elasticity of the central fiber than the dried glue coat (Fig. 2G). This is very similar to previous observations on the giant piriform fibers of gnaphosid spiders and suggests that the different properties (strong vs. elastic) of the two phases act synergistically in producing an overall high toughness (Wolff et al. 2017a). Beads-on-a-string structures on forcibly silked piriform fibers (Fig. 2F) showed that the initially fluid glue coat has viscoelastic properties before it dries. Previous tensile tests have demonstrated that piriform silk may be highly elastic and is much more extensible than the ampullate silk of draglines at a similar toughness (Wolff et al. 2017a; Greco et al. 2020).

3.1.2. General spinning kinematics

The basic pattern of anchor spinning was consistent across all species studied. Before and after each sequence the spinnerets were widely spread (Figs. 4A,C). If a dragline was not yet present, it was initiated by rubbing the anterior lateral spinnerets against each other or by sweeping the spinnerets over the substrate. This visibly triggered the silk flow and led to a white globular or tubular mass of piriform and major ampullate silk. In some cases, the rubbing was also performed, if a dragline was already present and usually was the start of the dragline envelope and bridge (Fig. 4B), which was then set onto the substrate and continued by the following sweeping movements. This initiation behavior was followed by a set of stereotypic sweeping movements (abduction-adduction cycles), which we called *kinematic motifs* (Figs. A,C,E,F). During this phase, the anterior lateral spinnerets applied piriform silk material onto the substrate. The ‘sweeping’ on the substrate was usually performed by both anterior lateral spinnerets alternately, i.e. when the left spinneret was abducted the right one was adducted, although in some instances abduction cycles were simultaneous or with shifted phases. The shape of the kinematic motifs was highly affected by phylogenetic history and usually more conserved in aerial web spinners than in hunting spiders and basic web spinners (Wolff 2021). Anterior lateral spinneret movements were often accompanied by regular movements of the posterior median spinnerets, and in some cases by the posterior lateral spinnerets. In these cases, the posterior spinnerets added silk material (presumably minor ampullate and aciniform silks) to the anchor (described in detail in another paper; Wolff 2020). The regular movements of the spinnerets were often combined with lateral and longitudinal body movements (see section 3.2.3.).

3.1.3. Intraspecific plasticity and disparate spinning behavior

An experimental approach has previously demonstrated that the spinning of dragline anchors is stereotypic and rather the size is adjusted towards different needs than the overall structure and geometry (Wolff et al. 2018). However, there are some reports of species being able to produce distinct types of anchors that serve different functions. Cobweb spiders (Theridiidae) use different anchor architectures for structural line attachments ('scaffold discs') and for pre-stressed capture threads that come off upon prey contact ('gumfoot discs') (Sahni et al. 2012). The easier breakage of the gumfoot disc is achieved by a weakened bridge rather than by different fiber orientations (Wolff 2017). We found similar disparate anchor architectures in *Pholcus phalangioides* (Pholcidae), which independently evolved a cobweb with gumfoot threads. In this case, the gumfoot disc was a strongly reduced anchor, consisting of simply a small deposit of the piriform glue mass. Another special architecture is the 'stilt anchor' of *Uroctea* sp. (Oecobiidae) (Kullmann and Stern 1975) and some Segestriidae (Foelix 2011): here a piriform bridge is reinforced and elevated, so that it suspends the dragline above the substrate, which is only used for the building of special stumbling lines. In many hunting spiders we observed that anchors used to attach lines of silken shelters were larger and denser than usual dragline anchors and occasionally exhibited a disparate shape. This may also be true for anchors used in webs, but a systematic comparison was not performed.

3.2. Interspecific differences and evolutionary trends

3.2.1. Systematic description of anchor structure and spinning behavior

A systematic and illustrated comparative description of anchor structure, dragline use and spinning behavior can be found in the electronic supplemental material (S2). Figures 5-13 display the results for exemplary species grouped in clades covering the major diversity and modifications of anchor structure, spinning kinematics, spinning apparatus morphology and their interplay, as described in the following.

3.2.2. Evolution of structural characters of silk anchorages

Straight dragline. Ancestral character estimation (ACE) strongly supported that a straight dragline is the derived character state of dragline fiber arrangement (Fig. 2). It evolved at an asymmetric rate (*AICcW*=0.983 for the ARD model) with an estimated 23 origins and no losses.

Dragline envelope. ACE results indicate that the dragline envelope is a derived trait that evolved at equal rates (*AICcW*=0.620 for the ER model) with an estimated 11 gains and 3 losses.

Dragline suspension (bridge). ACE suggests that the bridge evolved at equal rates (*AICcW*=0.736 for the ER model) with an estimated 18 gains and 8 losses.

Split plaque. The plaque was usually a single structure, however, in some species each ALS formed a separate plaque and the dragline was not bundled. This was most extreme in spiders in which the ALS were strongly separated, such as in the Oecobiidae (Figs. 10A,E,F) and Hahniidae (Fig. S2.4d), but was also observed in the Titanoecidae (*Goeldia* sp., Figs. S2.2a,b), Dysderidae (*Harpactea rubicunda*, Fig. S2.1t) and some Segestriidae (only some *Ariadna* spp., Fig. S2.1o) and Eresidae (occasionally in *Eresus* sp.). In all these cases the split plaque is an apomorphic and convergent character state.

Increase of piriform glue fraction. The piriform glue coat is usually so thin that it is not distinguishable from the piriform fiber with a light microscope (for exception see Fig. S2.3jj). However, in some cases the glue spreads out widely between fibers and on the substrate, indicating larger glue amounts. This was observed in some Theridiidae (e.g. Fig. S2.2w), which is further supported by previous ultrastructural analyses (Wirth et al. 2019). In some cases, the glue trails were highly enlarged, most noteworthy in the Pholcidae (Figs. 5L and S2.1x-cc), many Gnaphosidae and some Trochanteriidae (*Hemicloea* sp., Fig. S2.3ss). In these cases, piriform silks were also used in a foraging context (Japyassú and Macagnan 2004; Wolff and Gorb 2016; Wolff et al. 2017a).

Plaque shape. The plaque may have different shapes, e.g. circular or rectangular. Cribellar and more basic lineages tended to spin wider plaques with the primary fiber orientation being orthogonal towards the median axis.

Loading point position. There was a repeated evolutionary trend of shifting the position of the loading point towards the center of the plaque, which has consequences for anchor strength – this was discussed in detail in a previous paper (Wolff et al. 2019).

3.2.3. Evolution of spinning behavior

Spinning speed. There was a repeated evolutionary trend towards shorter times needed to produce an anchor. This is described in detail in another paper (Wolff 2021).

Contribution of the posterior spinnerets. The phylogenetic distribution of spinneret involvement was described in detail in another paper (Wolff 2020). We found that in species in which posterior spinnerets were active, they performed periodic movements with a similar

353 frequency as the anterior lateral spinnerets, although the exact choreography was usually
354 different from that of the anterior lateral spinnerets (e.g. Figs. 5J,O).
355 *Spinneret movement patterns*. The shapes of spinneret movement tracks were mostly
356 stereotypic and contained phylogenetic signatures. This is described in detail in Wolff (2021).
357 *Longitudinal body movement*. In most species, consecutive kinematic motifs were
358 placed along a longitudinal gradient, i.e., the opisthosoma was slightly moved forward while
359 spinning. This affects the plaque shape, which increases in length as the body moves forward.
360 A special behavior is a back-and-forth body movement, i.e. the opisthosoma is first gradually
361 moved forwards and then shortly backwards (e.g. Fig. 13I). This shifts the loading point more
362 towards the plaque center and reinforces the upstream bridge (Wolff and Herberstein 2017).
363 This behavior was observed in most araneoids (i.e. in all araneoid species tested except
364 Mimetidae; in Linyphiidae ambiguous state) and – as a convergent character – in the large New
365 Zealand sheet web spider *Cambridgea foliata* (Desidae).
366 *Lateral body movement*. The opisthosoma was often slightly moved laterally along with
367 the abduction-adduction cycles of the anterior lateral spinnerets, which enhanced lateral
368 displacements of the anterior lateral spinneret tips. However, in some clades the opisthosoma
369 was not moved laterally (e.g. Segestriidae (Fig. 5J), Agelenidae (Fig. 7J), Oecobiidae (Fig.
370 10I), Arkyidae (Fig. 13T)). In contrast, in some species the lateral movements were solely
371 performed by the opisthosoma and the anterior lateral spinnerets were only performing
372 longitudinal movements (in Hersiliidae (Fig. 10J), Zodariidae (Fig. 10P) and *Tasmanoonops*
373 (Orsolobidae, Fig. 5P)). These are considered apomorphic conditions.
374
375 *3.2.4. Evolution of spinneret shape*
376 The piriform silk used for anchor building is spun from a spigot field on the anterior
377 lateral spinnerets, which also bear the major ampullate gland spigots (Eberhard 2010). The
378 relative position of the major ampullate spigot towards the piriform spigot field might be a
379 major determinant of the dragline joint structure. For instance, in the Filistatidae, Eresidae and
380 Zodariidae the major ampullate spigots are interspersed in the piriform spigot field (Platnick et
381 al. 1991; Ramírez et al. 2014), which explains that in the anchors of these species the major
382 ampullate fibers followed the same looping patterns as the piriform fibers (Figs. 5F, S2.1i-m,
383 S2.2k-m, S2.3a). In contrast, in most other araneomorphs the major ampullate spigots are
384 located on a separate proximal partition of the spinneret tip (Coddington 1989; Murphy and
385 Roberts 2015) (e.g. Figs. 8C, 13C,K,M), which means that the major ampullate fibers are rather

deposited in the central part of the anchor and their spinning is rather independent of the deposition of the piriform fibers.

In our μCT analysis, we found that the shape of the anterior lateral spinnerets is usually conical, with varying length. Some clades evolved cylindrical spinnerets, especially the Filistatidae (Figs. 5A-B), Miturgidae (Figs. 8C-D), Gnaphosoidea (Figs. 9A-D) and Oecobiidae (Figs. 10A-B). In the Gnaphosidae the modification of the spinneret into a long rigid tube may enhance pressure regulation to enable a special piriform gland activation mechanism (Wolff et al. 2017a). In *Molycria mammosa*, the modification was most extreme: the cylindrical anterior lateral spinnerets were extremely elongated and their basic articulation was shifted far anteriorly (Figs. 9C,D). This is a special adaption towards the directed use of piriform silk in prey capture (Fig. 9G), which is a unique feature of Gnaphosoidea (Wolff et al. 2017a; Baydizada et al. 2020).

The tip of the anterior lateral spinneret bearing the spigot field was a flexible, poorly sclerotized plate that was either flat (most species) or curved. Strongly curved spigot fields were found in Austrochilidae (*Hickmania troglodytes*, Fig. 6B) and Araneidae (*Argiope keyserlingi*, Fig. 13D, and *Trichonephila plumipes*) .

3.3. Joint effects of morphology and behavior on anchor structure

3.3.1. Relationship between spinneret shape, spinning choreography and dragline joint structure

Our integrative study revealed a direct link between the spinning patterns and the arrangement of piriform fibers in the plaque. Furthermore, kinematic patterns also affect the plaque geometry and loading point position (Wolff et al. 2019). There is a general notion that behavioral evolution has more degrees of freedom and is more variable and homoplasic than the evolution of morphology, however empirical evidence is ambiguous (supporting, e.g. Blomberg et al. 2003; Eberhard et al. 2008; Ord and Summers 2015; rejecting, e.g. de Queiroz and Wimberger 1993; Wiens 2000). We note that the evolution of spinning behavior is constrained by the morphology of the spinning apparatus (see 3.3.2. below) and thus does not evolve independently.

We had initially assumed that the structure of the dragline joint, especially the bridge, requires a modification of the spinneret tip shape. Contrary, we found that across species, spinneret morphology (major ampullate spigot position and piriform spigot field shape) did not correlate with dragline joint structure. For instance, looped dragline fibers were found in spiders, in which the major ampullate spigots were interspersed in the piriform spigot field

(*Kukulcania hibernalis*, Figs. 5A-B,F, *Stegodyphus dumicola*, Figs. 12A-B,F), but also in species, in which those spigot types were clearly separated (e.g. *Kaiya terama*, Figs. 6C-D,H, *Amaurobius fenestralis*, Figs. 7A-B,F, *Oncodamus bidens*, Figs. 12C-D,H). Also, a curved piriform spigot field was not required for the construction of neither a dragline envelope nor a bridge. Curved spigot fields were only found in araneids, which are nested within a group of spiders most of which built bridge joints (Fig. 13), and in the austrochilid *Hickmania troglodytes*, whose anchors exhibited a dragline envelope but no bridge (Figs. 6A-B,F). However, modified dragline joints were produced by far more species.

We found that the way how the spinnerets were moved towards each other played an important role in the formation of the dragline joint. In species that constructed a dragline envelope and/or bridge both anterior lateral spinnerets met in between each sweeping movement. When doing so, the distal articles were expanded, so that the spigot fields faced each other, and then rubbed along each other. We assume that depending on whether this rubbing is performed in the proximal-distal, anterior-posterior or both directions, either a bridge, a dragline envelope or both is formed. In species in which the dragline fibers were directly incorporated into the plaque, the anterior lateral spinnerets usually did not meet and remained in substrate contact throughout the whole sequence. Again, it should be noted that the described movements are dependent on morphology, in particular the location of pivot points between spinneret articles and the ratio between sclerotized versus membranous parts in the distal article. This and differences in muscular equipment remain to be investigated in detail in the future.

3.3.2. Effect of the presence of a cribellum organ

The cribellum is a spinning plate that is used to produce dry adhesive capture threads (Opell 2013). It is synapomorphic to araneomorph spiders and was repeatedly lost at different time points of spider evolution (Miller et al. 2010). We found that the cribellum mechanically constrains the mobility of the anterior lateral spinnerets. In particular, anterior directed movements of the anterior lateral spinnerets may be blocked by the cribellum organ. This results in relatively similar spinning patterns dominated by lateral abductions across a range of distantly related cribellar species (Figs. 5E, 6E, 7E, 11E,G, 12E).

Anterior directed movements may heavily enhance anchor function by extending the glue application beyond the loading point, which reduces stress concentrations in the plaque and delays anchor detachment under load (Wolff et al. 2019). Generally speaking, our results suggest that the loss of the cribellum permitted more anterior directed movements of the

anterior lateral spinnerets, which facilitated an improvement of anchor function. This can be best understood when comparing the spinning patterns and anchor structures of related cribellar and ecribellar species (e.g. in Figs. 5 and 12; but see Fig. 6 for a case in which spinning patterns did not change after cribellum loss). The marronoid clade appears to be an exception, among which modified spinning patterns emerged without a loss of the cribellum (Fig. 7). In these cases, the anterior lateral spinnerets evaded the reduced mobility by enhancing the posterio-lateral abductions (Figs. 7O,S).

3.4. Does anchor structure reflect spider ecology?

3.4.1. Correlation between web type and anchor structure

Anchors with dragline envelope and bridge (considered the most derived type of anchor architecture) were almost exclusively found in spiders that build aerial webs, such as orb web spiders, or semi-aerial webs (i.e. webs with a substrate bound tubular retreat and a large aerial sheet). This included the majority of araneoids (Fig. 13), but also the Deinopidae and most Uloboridae (Fig. 11), some Desidae (*Badumna* spp., Figs. 7G, S2.4dd-ee, Porteriinae, Figs. S2.4gg-kk), the Psechridae (*Psechrus* sp., Fig. S2.3g) and the web building representatives of Pisauridae (*Dendrolycosa icadia*, Fig. S2.3h) and Gradungulidae (*Progradungula* sp., Fig. S2.1f). Especially in the latter three cases, the correlation of that trait with the web building ecology is most apparent as their web-less sister lineages do not exhibit anchors with these characters. The only hunting spiders in which the bridge+envelope condition was observed (*Scytodes thoracica* (Scytodidae), Fig. S2.1r; Mimetidae spp., Figs. S2.2aa-bb; *Goyenia* cf. *fresa* (Desidae), Fig. S2.4ff) were direct descendants of web building lineages. This suggests that this modification of the dragline joint is an adaptation towards the building of large suspended webs. A major advantage of this modification might be an enhancement of the anchor resistance towards tensile loads under varying angles by the reduction of stress concentrations. In some cases, the silk envelope may also have the function to prevent a catastrophic failure by representing a predetermined breaking point: a previous biomechanical study showed that in orb web spiders the envelope acted like a sheath and was responsible for a special failure mode, where the dragline-piriform silk interface broke leading to the dragline sliding through the otherwise intact anchor under the generation of friction (Grawe et al. 2014). This may also play a role in so-called ‘sliding junctions’ that prevent the breakage of orb webs at the interface of stiff and elastic lines (Eberhard 1976).

The aberrant anchors of Pholcidae with their large amounts of glue stand in relationship with the secondary use of the piriform silk for prey capture and defense in this family (Wolff

and Gorb 2016). Such anchors might not be very economic to produce and mechanically less efficient; however, the use of piriform glue in prey immobilization enables these spiders to capture large and dangerous prey, which may outweigh any costs related to this anchor modification.

3.4.2. Loss of silk anchors and functional shifts of piriform silk use

Among araneomorph spiders there are only few instances, where silk anchors have been lost. In most Gnaphosoidea, especially the Gnaphosidae s.str. and Molycriinae (Fig. 9), but also some Lamponidae and Trochanteriidae (Figs. S2.3tt,uu), draglines and anchor spinning behavior were absent and piriform silk was primarily used for prey capture (see Wolff et al. 2017a for details). Many gnaphosids spin silken shelters, which may be attached with deposits of piriform silk, but these were never placed in a regular shape and not connected with a dragline, and thus were not consider true silk anchors (Wolff et al. 2017a). *Arboricaria sociabilis* was found to be a rare case of a gnaphosid that used a dragline, but the anchor was also of an irregular shape (Fig. S2.3vv).

In *Loxosceles* spp. (Sicariidae) major ampullate silk has evolved into a dry adhesive and is not used for draglines (Magalhães et al. 2017). Accordingly, silk anchors were extremely rare in these spiders (for details see S2). Spiders of some related families (Diguetidae, Plectreuridae) have strongly reduced or even absent piriform spigot fields (Platnick et al. 1991). We did not have access to specimens from these families, so it remains unclear how these taxa anchor their lines and webs. Draglines and regular anchors were also mostly absent in the Zodariidae (Figs. 10M,N) and some Miturgidae, which rather used the piriform silk to produce substrate sheets (for details see S2). These may be adaptations towards a ground living ecology and the sole use of piriform silk in the construction of substrate-bound shelters.

3.5. Evolutionary enhancement of the mechanical robustness of attachment discs

It was previously demonstrated that the silk anchor architecture strongly affects the anchor's resistance against tensile loads (Sahni et al. 2012; Pugno et al. 2013; Wolff and Herberstein 2017) and that there was a repeated evolutionary trend towards a more efficient geometry (Wolff et al. 2019). The evolutionary changes in dragline joint structure described here may also represent adaptations towards enhanced anchor function. For instance, dragline bundling and the adding of an elastic bridge could enhance energy dissipation and robustness towards steep loading angles. This is a subject for future biomechanical studies. The adding of silk from posterior spinnerets to the anchor may be a way to tailor the mechanical properties

of the plaque. For instance, by combining strong and elastic fibers, the overall toughness of the silk compound could be enhanced. However, so far, this is hypothetical and requires further investigation.

It is very probable that the evolutionary enhancement of anchor function is under a stronger selective pressure in certain ecological guilds (esp. aerial web builders) than in others (e.g. ground runners), and that it happened not gradually but rather in jumps (Wolff et al. 2019). Such jumps could be enabled by pointed morphological changes such as the loss of the cribellum organ, if coinciding with a strong selective pressure on anchor function. This highlights the relationship between morphological and behavioral change in the evolution of extended phenotype functions.

4. Conclusions

Here we have demonstrated differences and evolutionary trends in the structure of spider silk anchors. An integrative approach was adopted to reveal the concerted effects of behavior and morphology on the architecture of the extended phenotype product.

The major findings are summarized in the following:

1. The architecture of silk thread anchorages is dependent on the evolutionary history of the spider, but multiple homoplasies exist.

2. Anchor architectures with bundled, enclosed and suspended dragline fibers are apomorphies that evolved repeatedly, often in close association with aerial webs. These may be enhancements of the anchor function.

3. There was a repeated evolutionary trend in shifting the dragline exit point towards the plaque center, creating more robust anchorages. This trend was often accelerated by the loss of the cribellum organ that constrains the mobility of the anterior lateral spinnerets.

4. The above evolutionary trends in anchor architecture were mostly explained with changes in the innate spinning choreography and not with the shape of the spinneret tip nor the arrangement of spigots.

5. Reduction or losses of dragline anchorages were rare evolutionary events in araneomorph spiders, highlighting the broad utility of these silk structures. The use of piriform silk in prey capture is a rare case that led to a radical modification or loss of silk anchors.

We conclude that predominately the evolution of constructing behavior leads to changes in anchor architecture, but it is leveraged by morphological change. This highlights the role of morphology in the evolution of behavior and extended phenotypes. By revealing the evolutionary trends of anchor structure, this study also provides a roadmap for the choice of biomimetic models that may inspire new instant line attachments for industrial and household applications (Wolff 2017). For this purpose, there is a need for biomechanical and numerical approaches to better understand the function of envelope and bridge joints in spider silk anchorages.

Acknowledgements

We are grateful to Steffen Bayer, Niall Doran, Stanislav Gorb, Arno Grabolle, Siegfried Huber, Anna-Christin Joel, Alex Jordan, Ajay Narendra, Bryce McQuillan, Robert Raven, Milan Řezáč, Wolfgang Schlegel, Axel Schönhofer, Cristina Scioscia, Gabriele Uhl, Cor Vink and Sylvia Voss for providing resources and advice. We are grateful to Helen Smith and Graham Milledge for advice on Australian fieldwork and help with species identification. We thank Ingi Agnarsson and an anonymous reviewer for providing constructive comments on our manuscript.

This study was supported by a Macquarie University Research Fellowship of Macquarie University and a Discovery Early Career Researcher Award of the Australian Research Council [DE190101338] to JOW. JOW thanks the MQ Microscopy Unit, Sue Lindsay and Nicole Vella, for experimental support with FESEM imaging.

Data accessibility

Detailed descriptions and illustrations of silk anchors and the character matrix are deposited in the electronic supplemental material (S2 and S3).

References

Baydizada N, Tóthová A, Pekár S. 2020. Tracing the evolution of trophic specialisation and mode of attack behaviour in the ground spider family Gnaphosidae. Org Divers Evol. 20(4):551-563.

Blomberg SP, Garland Jr T, Ives AR. 2003. Testing for phylogenetic signal in comparative data: behavioral traits are more labile. Evolution. 57(4):717-745.

Coddington JA. 1989. Spinneret silk spigot morphology: evidence for the monophyly of orbweaving spiders, Cyrtophorinae (Araneidae), and the group Theridiidae plus Nesticidae. J Arachnol. 17(1):71-95.

Dawkins R. 1982. The extended phenotype: The long reach of the gene. Oxford: Oxford University Press.

de Queiroz A, Wimberger PH. 1993. The usefulness of behavior for phylogeny estimation: levels of homoplasy in behavioral and morphological characters. Evolution. 47(1):46-60.

Diikstra H. 1976. Searching behaviour and tactochemical orientation in males of the wolfspider *Pardosa amentata* (Cl.) (Araneae, Lycosidae). Proceedings of the Koninklijke Nederlandse Akademie Van Wetenschappen-Amsterdam Series C. 79:235-244.

Eberhard WG. 1976. Physical properties of sticky spirals and their connections: sliding connections in orb webs. J Nat Hist. 10(5):481-488.

Eberhard WG. 2010. Possible functional significance of spigot placement on the spinnerets of spiders. J Arachnol. 38(3):407-414.
Eberhard WG, Agnarsson I, Levi HW. 2008. Web forms and the phylogeny of theridiid spiders (Araneae: Theridiidae): chaos from order. System Biodivers. 6(4):415-475.
Eberhard WG, Hazzi NA. 2013. Web construction of *Linothele macrothelifera* (Araneae: Dipluridae). J Arachnol. 41(1):70-75.
Foelix RF. 2011. Biology of spiders. Oxford, New York: Oxford University Press.
Grawe I, Wolff JO, Gorb SN. 2014. Composition and substrate-dependent strength of the silken attachment discs in spiders. J R Soc Interface. 11(98):1742-5662.
Greco G, Wolff JO, Pugno NM. 2020. Strong and tough silk for resilient attachment discs: the mechanical properties of piriform silk in the spider *Cupiennius salei* (Keyserling, 1877). Front Mater 7:138.
Japyassú HF, Macagnan CR. 2004. Fishing for prey: the evolution of a new predatory tactic among spiders (Araneae, Pholcidae). Revista de Etologia. 6(2):79-94.
Kovoor J, Zylberberg L. 1980. Fine-structural aspects of silk secretion in a spider (*Araneus diadematus*). 1. Elaboration in the pyriform glands. Tissue Cell. 12(3):547-556.
Kullmann E, Stern H. 1975. Leben am seidenen Faden. München: Bertelsmann.
Magalhães I, Ravelo A, Scioscia C, Peretti A, Michalik P, Ramírez M. 2017. Recluse spiders produce flattened silk rapidly using a highly modified, self-sufficient spinning apparatus. J Zool. 303(1):27-35.
Meijering E, Dzyubachyk O, Smal I. 2012. Methods for cell and particle tracking. Meth Enzymol 504:183-200.
Miller JA, Carmichael A, Ramírez MJ, Spagna JC, Haddad CR, Řezáč M, Johannesen J, Král J, Wang X-P, Griswold CE. 2010. Phylogeny of entelegyne spiders: affinities of the family Penestomidae (new rank), generic phylogeny of Eresidae, and asymmetric rates of change in spinning organ evolution (Araneae, Araneoidea, Entelegynae). Mol Phylogenet Evol. 55(3):786-804.
Murphy JA, Roberts MJ. 2015. Spider families of the world and their spinnerets. York: British Arachnological Society.
Nyffeler M, Birkhofer K. 2017. An estimated 400–800 million tons of prey are annually killed by the global spider community. Sci Nat. 104(3-4):30.
Opell BD. 2013. Cribellar thread. Spider ecophysiology. Springer. p. 303-315.
Ord TJ, Summers TC. 2015. Repeated evolution and the impact of evolutionary history on adaptation. BMC Evol Biol. 15(1):137.
Platnick NI, Coddington JA, Forster R, Griswold C. 1991. Spinneret morphology and the phylogeny of haplogyne spiders (Araneae, Araneomorphae). Am Mus Novit. 3016:1-73.
Pugno NM, Cranford SW, Buehler MJ. 2013. Synergetic material and structure optimization yields robust spider web anchorages. Small. 9(16):2747-2756.
Ramírez MJ, Grismado CJ, Labarque FM, Izquierdo MA, Ledford JM, Miller JA, Haddad CR, Griswold CE. 2014. The morphology and relationships of the walking mud spiders of the genus *Cryptothele* (Araneae: Zodariidae). Zool Anz. 253(5):382-393.
Revell LJ. 2012. phytools: an R package for phylogenetic comparative biology (and other things). Meth Ecol Evol. 3(2):217-223.
Sahni V, Harris J, Blackledge TA, Dhinojwala A. 2012. Cobweb-weaving spiders produce different attachment discs for locomotion and prey capture. Nat Commun 3(1):1-7.
Schneider CA, Rasband WS, Eliceiri KW. 2012. NIH Image to ImageJ: 25 years of image analysis. Nat Methods. 9(7):671-675.
Wiens JJ. 2000. Decoupled evolution of display morphology and display behaviour in phrynosomatid lizards. Biol J Linn Soc. 70(4):597-612.
Wirth M, Wolff JO, Appel E, Gorb SN. 2019. Ultrastructure of spider thread anchorages. J Morphol. 280(4):534-543.
Wolff JO. 2017. Structural effects of glue application in spiders – What can we learn from silk anchors? In: Xue L, Heepe L, Gorb SN, editors. Bio-inspired structured adhesives. Dordrecht: Springer Science+Business Media. p. 63-80.
Wolff JO. 2020. The evolution of dragline initiation in spiders: multiple transitions from multi-to single-gland usage. Diversity. 12(1):4.
Wolff JO, Gorb SN. 2015. Adhesive foot pads: an adaptation to climbing? An ecological survey in hunting spiders. Zoology. 118(1):1-7.
Wolff JO, Gorb SN. 2016. Attachment structures and adhesive secretions in arachnids. Cham, Switzerland: Springer International Publishing.
Wolff JO, Grawe I, Wirth M, Karstedt A, Gorb SN. 2015. Spider's super-glue: thread anchors are composite adhesives with synergistic hierarchical organization. Soft Matter. 11(12):2394-2403.
Wolff JO, Herberstein ME. 2017. 3D-printing spiders: back-and-forth glue application yields silk anchorages with high pull-off resistance under varying loading situations. J R Soc Interface. 14:20160783.

Wolff JO, Jones B, Herberstein ME. 2018. Plastic material investment in load-bearing silk attachments in spiders. Zoology. 131:45-47.
Wolff JO, Little D, Herberstein ME. 2020. Limits of piriform silk adhesion—similar effects of substrate surface polarity on silk anchor performance in two spider species with disparate microhabitat use. Sci Nat. 107(4):1-10.
Wolff JO, Paterno GB, Liprandi D, Ramírez MJ, Bosia F, van der Meijden A, Michalik P, Smith HM, Jones BR, Ravelo AM et al. 2019. Evolution of aerial spider webs coincided with repeated structural optimization of silk anchorages. Evolution. 73(10):2122-2134.
Wolff JO, Řezáč M, Krejčí T, Gorb SN. 2017a. Hunting with sticky tape: functional shift in silk glands of araneophagous ground spiders (Gnaphosidae). J Exp Biol. 220:2250-2259.
Wolff JO, van der Meijden A, Herberstein ME. 2017b. Distinct spinning patterns gain differentiated loading tolerance of silk thread anchorages in spiders with different ecology. Proc R Soc B. 284:20171124.
Wolff JO. 2021. Evolutionary kinematics of spinneret movements for rapid silk thread anchorage in spiders. J Comp Physiol A. In Press. https://doi.org/10.1007/s00359-020-01453-3

Figure legends

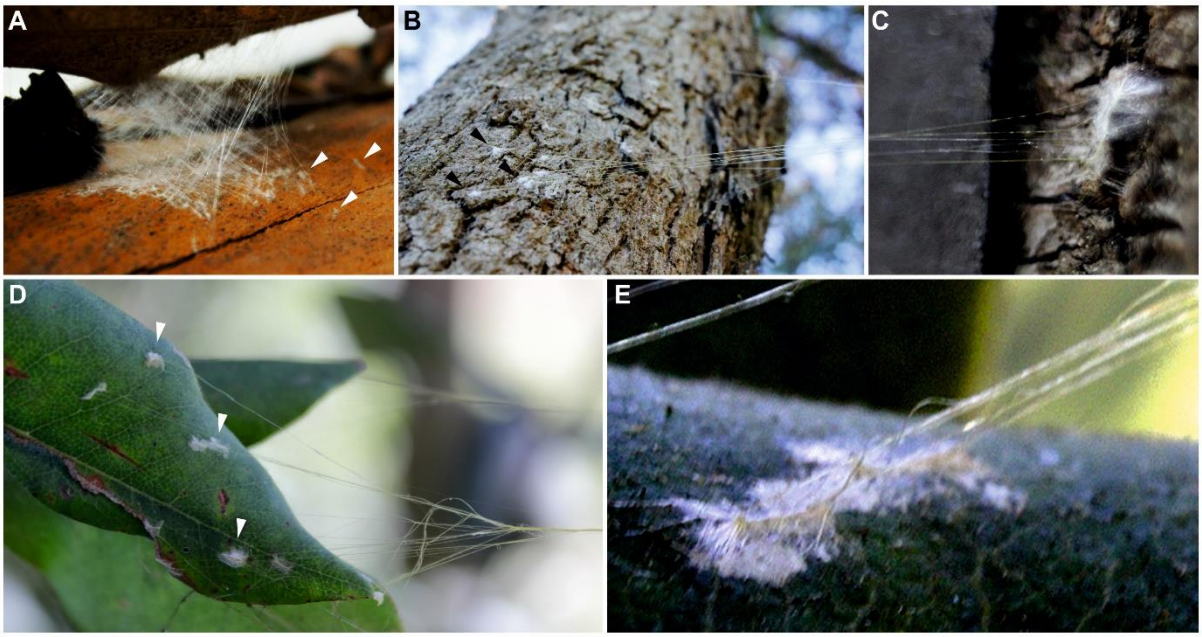

Fig. 1. Silk anchors in natural habitats. Macro photography of silk lines and silk anchors (arrowheads) on natural surfaces as found in the field in Sydney, Australia. (**A**) Attachments of the silk lining of a shelter spun by the hunting spider *Isopeda villosa* (Sparassidae) under loose bark of a Eucalypt tree. (**B**-**E**) Attachments of orb web anchor lines of the golden orb weaver *Trichonephila plumipes* (Araneidae) on tree bark and leaves. In *B* it can been seen that adhesion on leaves may be compromised by epicuticular wax layers (some anchors in the upper part are partly detached).

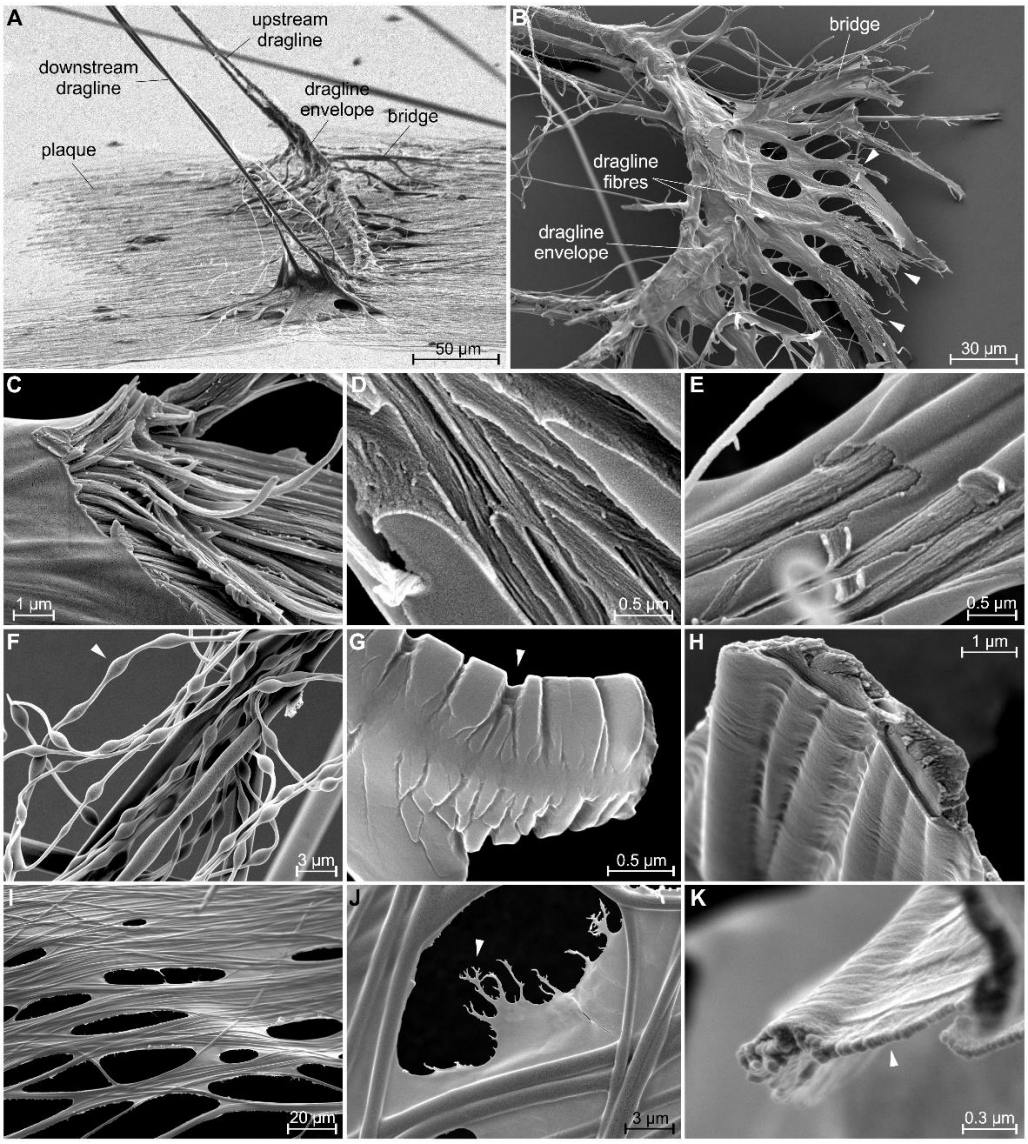

Fig. 2. Structure of silk anchors and piriform silk. Scanning electron micrographs of silk anchors. (**A**) SEM image of an attached dragline anchor of the cobweb spider *Steatoda sabulosa* (Theridiidae), different parts indicated. The upstream dragline is the end facing towards the spider (i.e. last spun), downstream vice versa. (**B-K**) FESEM images of fractured samples. (**B**) Bridge pulled out of a silk anchor of *Badumna longinqua* (Desidae) spun on glass. Arrowheads indicate fractures of piriform silk bundles. (**C**, **D**) Details of fracture faces of the piriform silk bundles of the bridge, as in *B*. (**E**) Fractured piriform silk of *Arachnura higginsi* (Araneidae). In this case two crossing layers of piriform silk fibers were separated, leading to the detachment of the glue phase from the fiber phase. (**F**) Piriform silk fibers and fiber bundles forcibly pulled from a *Trichonephila plumipes* (Araneidae). This was done by pushing a small paper frame between the spinnerets and the substrate during the production of an anchorage, so that some of the piriform silk was left as straight lines suspended across the frame. The missing substrate contact in the suspended fibers led to the glue coat forming beads-on-a-string structures (arrowhead) before solidification, demonstrating the viscoelastic nature of the piriform glue. (**G**) Stressed glue coat near the fracture site of a piriform silk fiber of *Eriophora* sp. (Araneidae). Fine cracks in the glue coat (arrowhead) are distributed in regular intervals and stopped in the middle, where the central fiber is situated. This indicates that the central fiber is more elastic than the glue coat, while the adhesion between both components is strong. (**H-K**) Fractured piriform silk of *Isopeda villosa* (Sparassidae). (**H**) Fracture face of piriform fiber array, showing the two-phasic structure. (**I**, **J**) Piriform silk film assembled on and delaminated from a hydrophobic surface (polypropylene film). Arrowhead in *J* shows the fringe-like edge of the glue coat that results from the water-repellence of the substrate removing the water-soluble compounds and leaving the larger proteinaceous fibrillar compounds behind. (**K**) Fracture face of a piriform silk fiber whose glue coat was in contact with a substrate surface (in contrast to *C-H*). The arrowhead points to the glue film resulting from the glue spreading on the substrate. Note the skin-core structure of the glue phase.

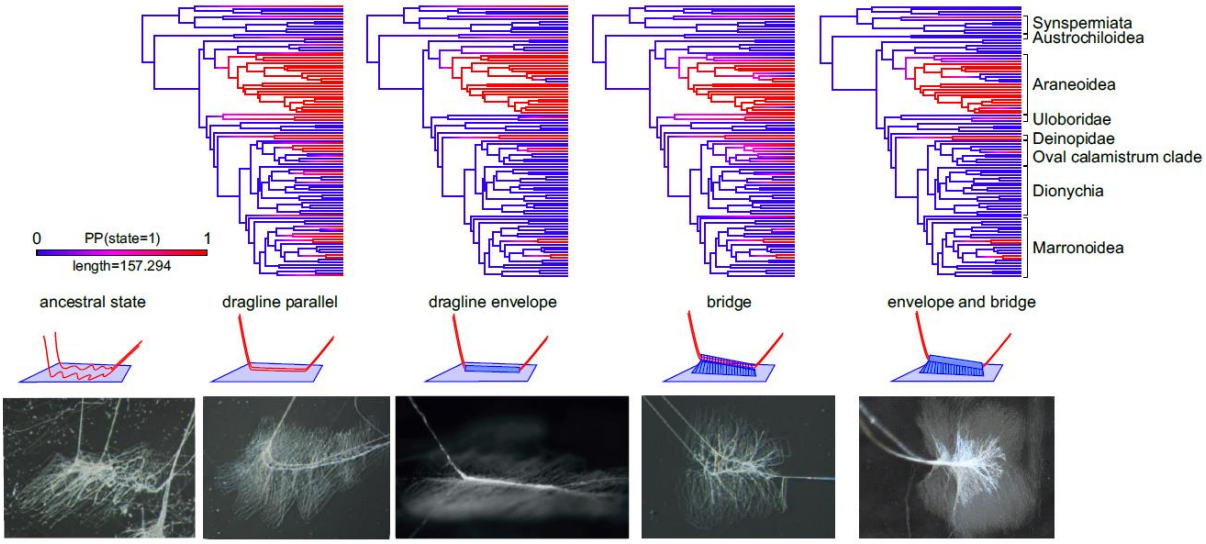

Fig. 3. Evolution of silk anchor structure. ContMaps (summary of 100 stochastic character mappings) of silk anchor characters, with blue indicating absence and red presence of the character. Character for each contMap visualized underneath with a schematic drawing and a micro-photograph of an exemplary anchor. The drawing and photo to the very left illustrate the ancestral state of the dragline joint, i.e. non-parallel, looped dragline fibers that are directly incorporated into the plaque. Note that the parallel dragline condition is the prerequisite for the dragline envelope and bridge. A bridge may or may not be combined with a dragline envelope.

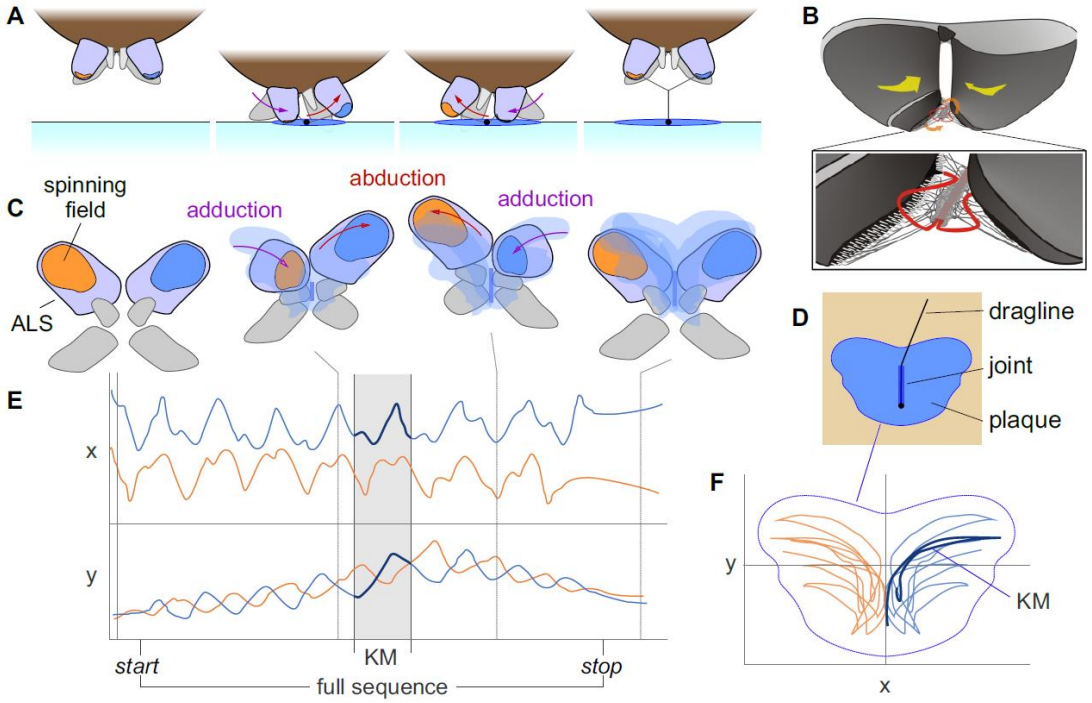

Fig. 4. Anchor spinning behavior. (**A**) Schematic illustration of anchor spinning sequence, as seen from anterior. Adapted from Wolff, 2021. (**B**) Schematic illustration of how the dragline envelope is formed by rubbing the spinning field of both ALS along each other (dragline fibers in red and piriform silk fibers in grey). (**C**) Sequence from *A*, as seen from ventral. (**D**) Schematic illustration of a discontinuous silk anchor. (**E**) x-t and y-t plots of spinning sequence as in *A* and *C* (vertical dotted lines indicate the time points illustrated above), showing the tracked position of both ALS spinning fields over time (blue line represents the left ALS and orange the right ALS, colored as in *A* and *C*). 'Start' and 'stop' mark the beginning and end of plaque production. The single kinematic motif is marked with a grey shade and thicker lines. (**F**) x-y plot of the full spinning track as in *E*. Single kinematic motif marked by thicker line. The blue dotted outline symbolizes the dimensions of the final anchor plaque (see *D*). **Abbreviations**: *ALS*, anterior lateral spinneret; *KM*, kinematic motif.

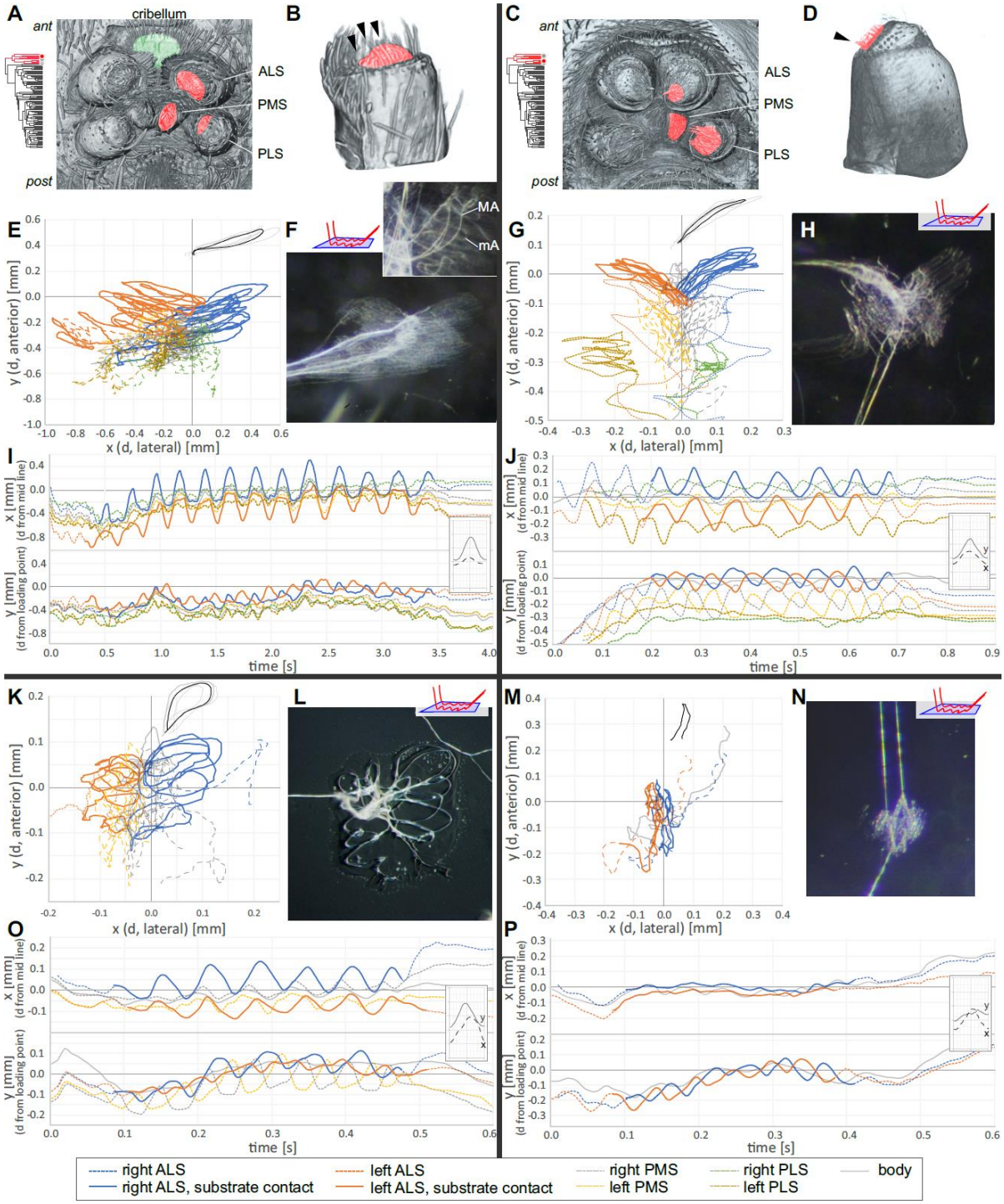

Fig. 5. Filistatidae and Synspermiata. (**A-B**, **E-F**, **I**) *Kukulkania hibernalis* (Filistatidae), cribellar web builder. (**C-D**, **G-H**, **J**) *Segestria florentina* (Segestriidae), ecribellar web builder. (**K-L**, **O**) *Pholcus phalangioides* (Pholcidae), ecribellar web builder. (**M-N**, **P**) *Tasmanoonops* sp. (Orsolobidae), ecribellar hunting spider. (**A-D**) 3D-reconstructions of spinnerets from µCT scans, with spinning fields of spinnerets colored in red, cribellum colored in green; *A* and *C*, ventral view; *B* and *D*, left anterior lateral spinneret, frontal view from anterior, arrowhead indicates position of major ampullate spigots. Red colored branches in small phylogeny next to figures indicate the clade the species from the figure are embedded in and red dot indicates the phylogenetic position of the displayed species. (**E**, **G**, **I-K**, **M**, **O-P**) Exemplary movement tracks of spinnerets active during the spinning of a silk anchorage, coordinates relative to upstream dragline exit point of silk anchor; *E*, *G*, *K* and *M* show x-y plots of the tracks (as in Fig. 4F), isolated kinematic motif shown above the full track, with the thin grey lines being the average of five tracks per individual and the black shape representing the global mean of 15 tracks from three individuals; *I*, *J*, *O* and *P* show the t-x plots (upper row) and the t-y plots (lower row) of spinneret movements

(as in Fig. 4E), the inset shows the mean x-d plots of the mean kinematic motif at the scale of the diameter of the ALS spinning field (black line x-direction and grey line y-direction); legend at the bottom of figure. (**F**, **H**, **L**, **N**) Light microscopy image of exemplary silk anchor on glass, same orientation as x-y-plots (i.e. anterior/upstream up). Compare with spinning plots to understand the differential origin of fibers seen in the microscopic image. Note in the anchor of *S. florentina* the silk from ALS, PMS and PLS forming distinct patches. Anchors of Pholcidae are special among all spiders in the plaque being a continuous film of glue as piriform glands in these spiders are highly enlarged. **Abbreviations**: *ALS*, anterior lateral spinneret; *ant*, anterior; *PLS*, posterior lateral spinneret; *PMS*, posterior median spinneret.

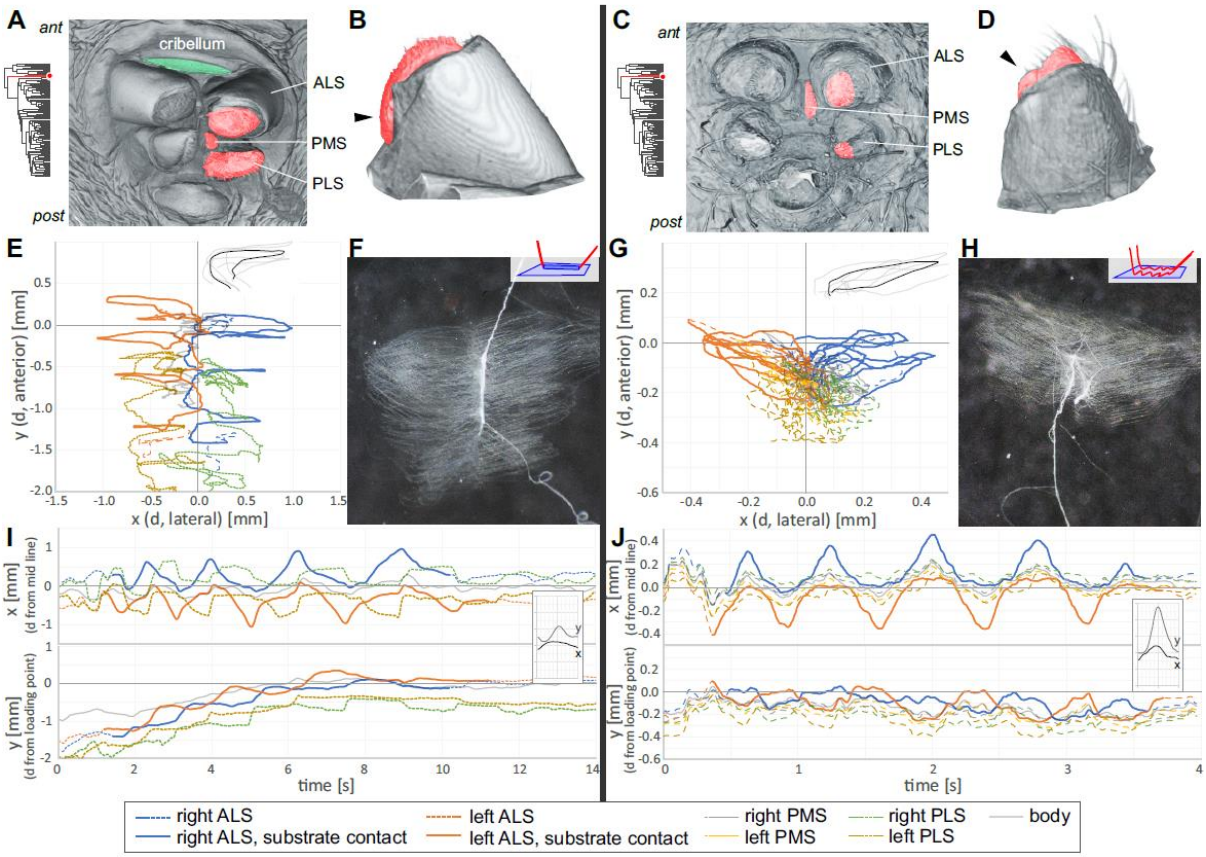

Fig. 6. Austrochiloidea. (**A-B**, **E-F**, **I**) *Hickmania troglodytes* (Austrochilidae), cribellar web builder. (**C-D**, **G-H**, **J**) *Kaiya terama* (Gradungulidae), ecribellar hunting spider. (**A-D**) 3D-reconstructions of spinnerets from µCT scans, same conventions as in Fig. 5. (**E**, **G**, **I-J**) Exemplary movement tracks of spinnerets active during the spinning of a silk anchorage (PMS not tracked in *H. troglodytes*, as barely visible), same conventions as in Fig. 5. (**F**, **H**) Light microscopy image of exemplary silk anchor on glass, same conventions as in Fig. 5. The anchor of *H. troglodytes* (**F**) exhibits a bundled dragline with an envelope but no bridge, while in *K. terama* (*H*) dragline fibers are separated and follow piriform fibers in the plaque.

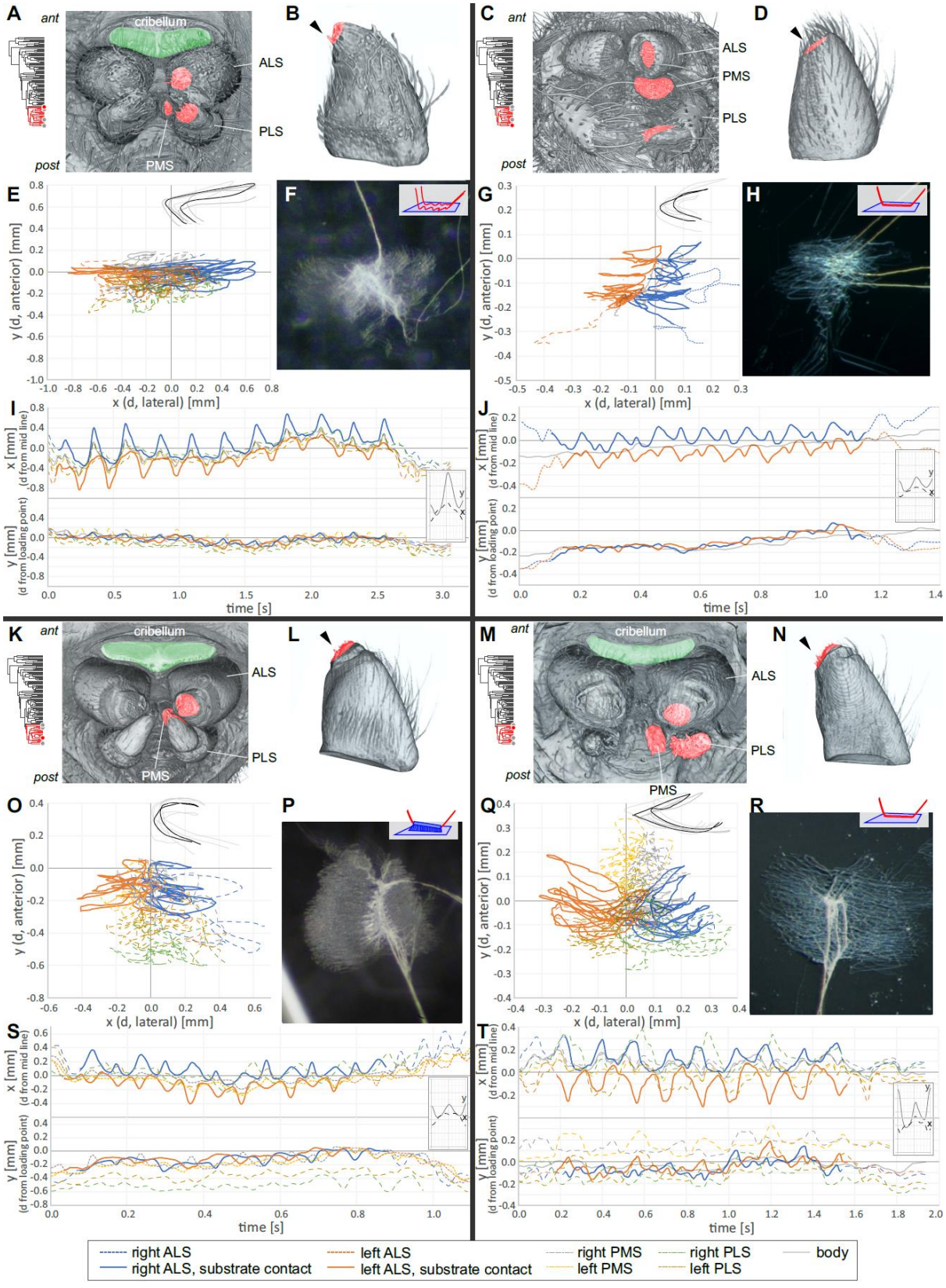

Fig. 7. Marronoidea. (**A-B**, **E-F**, **I**) *Amaurobius fenestralis* (Amaurobiidae), cribellar web builder. (**C-D**, **G-H**, **J**) *Tegenaria ferruginea* (Agelenidae), ecribellar web builder. (**K-L**, **O-P**, **S**) *Badumna insignis* (Desidae), cribellar web builder. (**M-N**, **Q-R**, **T**) *Therlinya vexillum* (Stiphidiidae), cribellar web builder. (**A-D**, **K-N**) 3D-reconstructions of spinnerets from µCT scans, same conventions as in Fig. 5. (**E**, **G**, **I-J**, **O**, **Q**, **S-T**) Exemplary movement tracks of spinnerets active during the spinning of a silk anchorage, same conventions as in Fig. 5. (**F**, **H**, **P**, **R**) Light microscopy image of exemplary silk anchor on glass, same conventions as in Fig. 5.

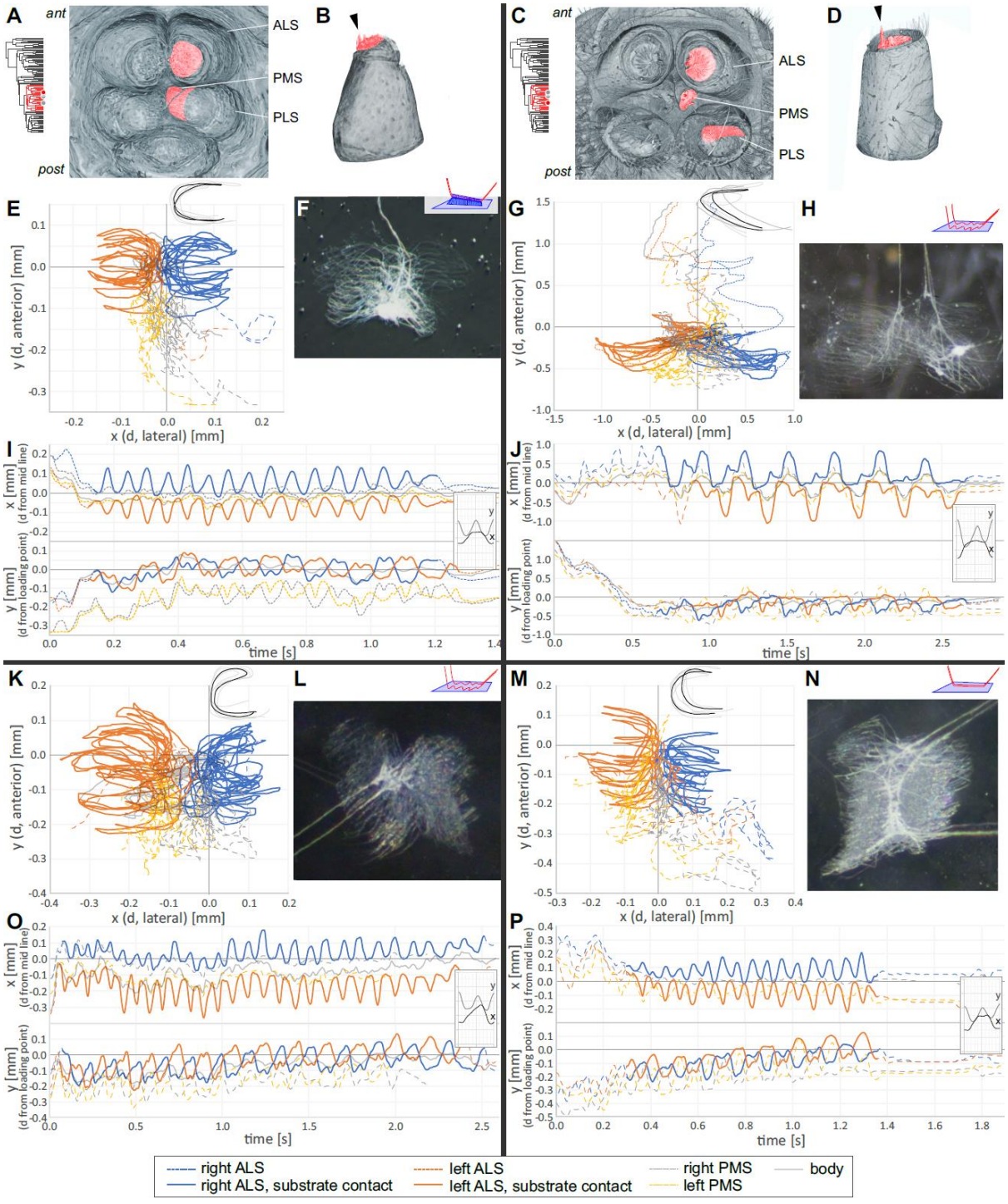

Fig. 8. Dionycha and Oval-calamistrum clade. (**A-B**, **E-F**, **I**) *Australomisidia* sp. (Thomisidae); (**C-D**, **G-H**, **J**) *Mituliodon tarantulinus* (Miturgidae); (**K-L**, **O**) *Oxyopes molarius* (Oxyopidae); (**M-N**, **P**) *Sandalodes superbus* (Salticidae), all ecribellar hunting spiders. (**A-D**, **K-N**) 3D-reconstructions of spinnerets from µCT scans, same conventions as in Fig. 5. (**E**, **G**, **I-J**, **K**, **O**, **M**, **P**) Exemplary movement tracks of spinnerets active during the spinning of a silk anchorage, same conventions as in Fig. 5. (**F**, **H**, **L**, **N**) Light microscopy image of exemplary silk anchor on glass, same conventions as in Fig. 5. Note that all except *N* show discontinuous dragline anchors (i.e. dragline initiations), but continuous dragline anchors (with in- and out-going dragline) are also produced by these species.

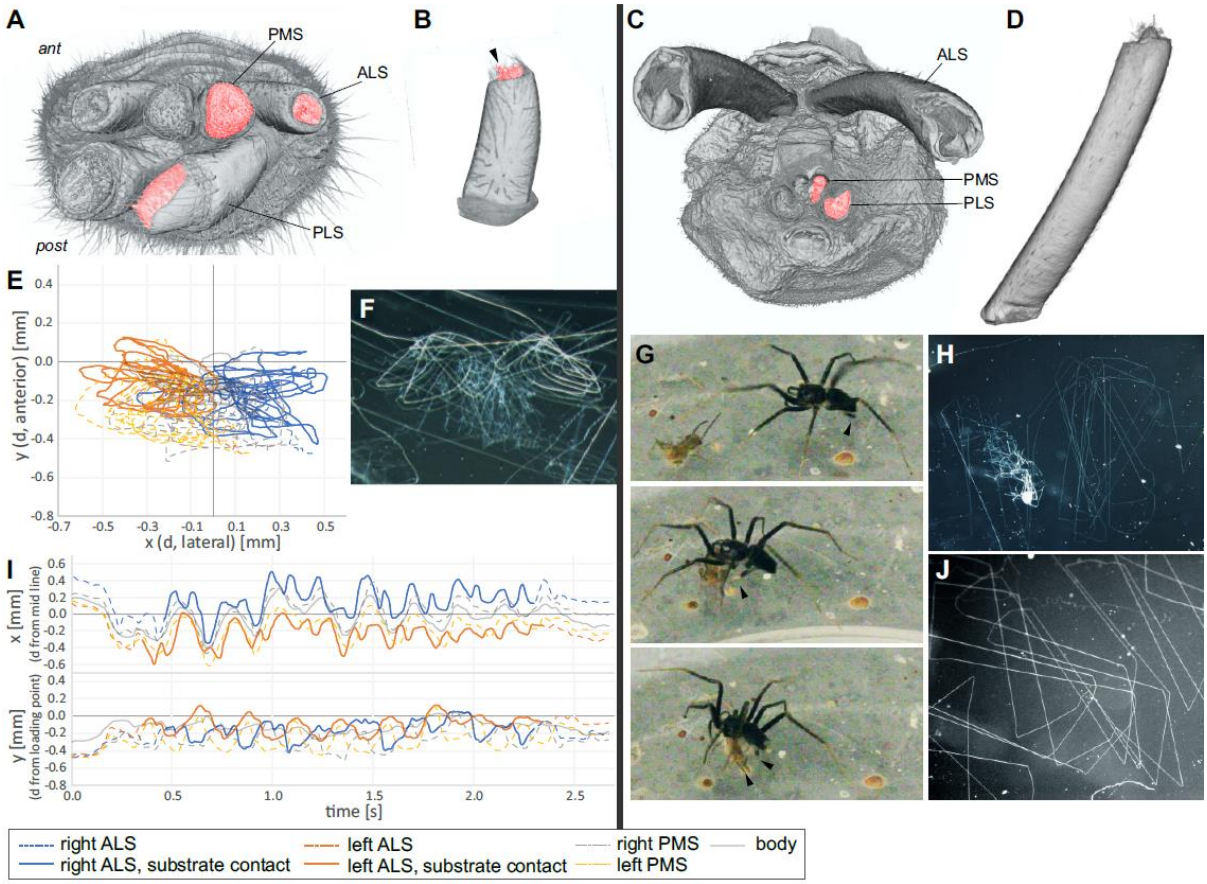

Fig. 9. Gnaphosoidea. (**A-B**, **E-F**, **I**) Lamponidae spec.; (**C-D**, **G-H**, **J**) *Molycria* sp. (Gnaphosidae), both ecribellar hunting spiders. (**A-D**) 3D-reconstructions of spinnerets from µCT scans, same conventions as in Fig. 5. Note that the ALS spinning fields are retracted in *Molycria* and thus not visible in its inactive state. (**E**, **I**) Exemplary movement tracks of spinnerets active during the spinning of a silk anchorage, same conventions as in Fig. 5. (**F**) Light microscopy image of exemplary silk anchor on glass, same conventions as in Fig. 5. Note the distinct deposition of silk from the PMS. (**G**) Frames of a video sequence recorded with a Canon EOS600D DSLR during the feeding of a *Molycria* sp. with a cricket nymph. Arrowheads point to the elongated ALS – note the lateral spreading and extreme anterior abduction of these spinnerets to immobilize the prey with piriform silk. (**H**, **J**) Light microscopy images of piriform silk trails left behind after a predatory attack. The whitish globule in *H* is a mass of piriform silk indicating the silk flow initiation, as similarly found in many discontinuous dragline anchors.

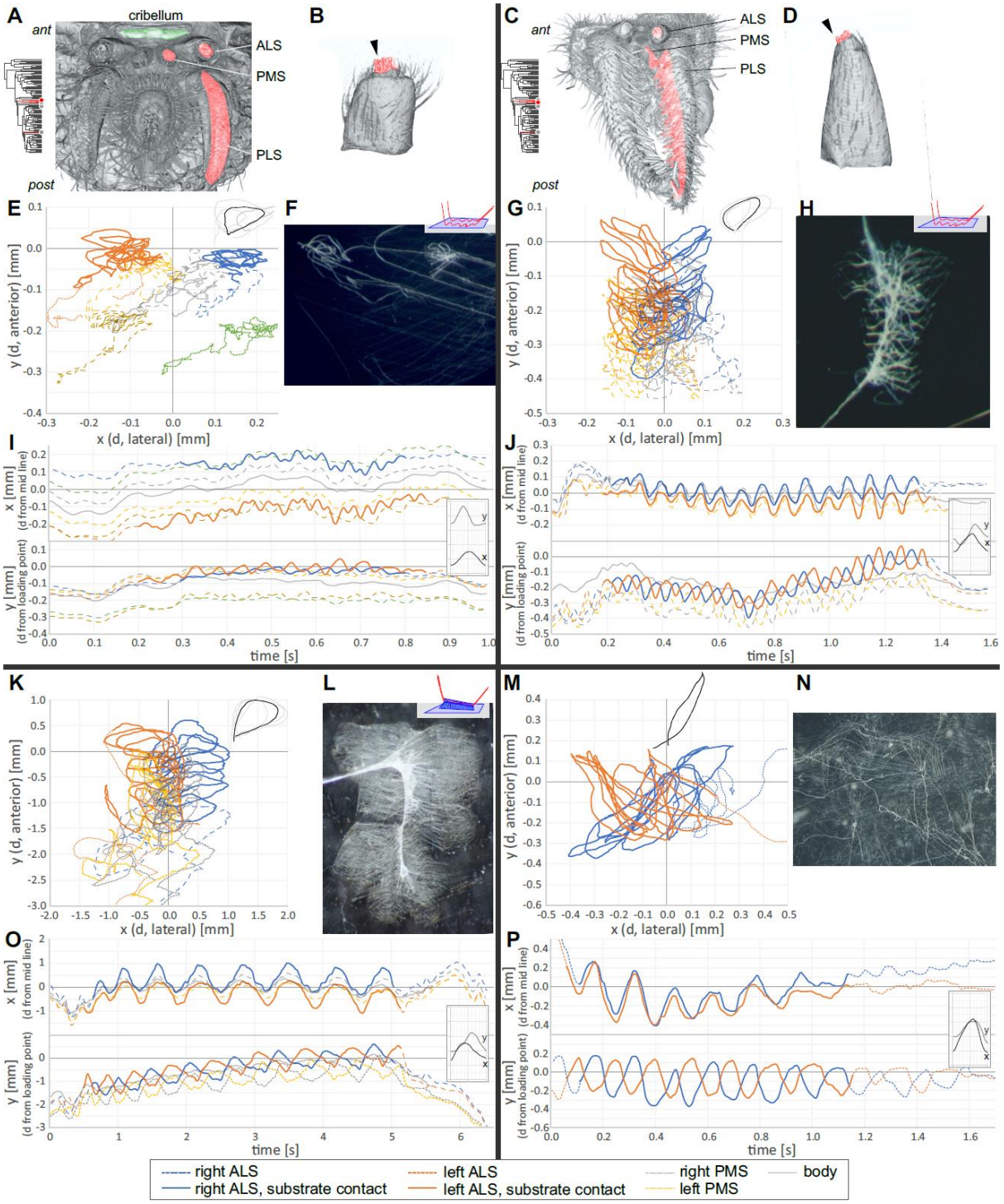

Fig. 10. Oecobioidea and basic RTA-clade. (**A-B**, **E-F**, **I**) *Oecobius navus* (Oecobiidae), cribellar web builder. (**C-D**, **G-H**, **J**) *Tamopsis* spp. (Hersiliidae), ecribellar web builder. (**K-L**, **O**) *Isopeda villosa* (Sparassidae), ecribellar hunting spider. (**M-N**, **P**) *Storena colossea* (Zodariidae), ecribellar hunting spider. (**A-D**) 3D-reconstructions of spinnerets from µCT scans, same conventions as in Fig. 5. (**E**, **G**, **I-K**, **M**, **O-P**) Exemplary movement tracks of spinnerets active during the spinning of a silk anchorage, same conventions as in Fig. 5. (**F**, **H**, **L**, **N**) Light microscopy image of exemplary silk anchor on glass, same conventions as in Fig. 5. Due to their specific spinneret arrangement, oecobiids spin a split plaque with spinnerets from each body side producing separate silk patches. Sparassids typically produce discontinuous dragline anchors (*L*). Zodariids do not produce clear anchors, but rather sheets (*N*, but see S2.3a,b for exceptions), *M* displays a part of a longer sequence where the spider performed similar spinning behavior in various positions on the substrate.

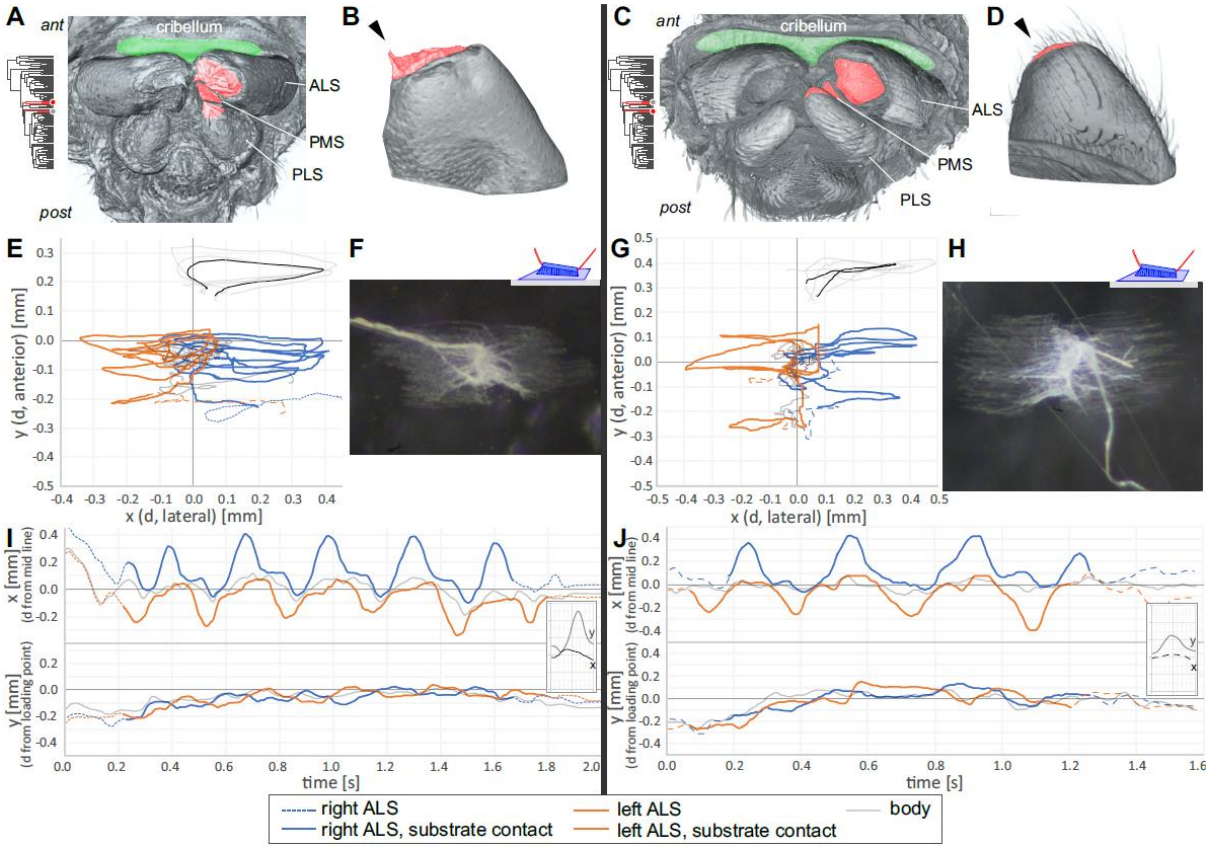

Fig. 11. Uloboridae and Deinopidae. (**A-B**, **E-F**, **I**) *Philoponella variabilis* (Uloboridae); (**C-D**, **G-H**, **J**) *Deinopis subrufa* (Deinopidae), both cribellar web builders. (**A-D**) 3D-reconstructions of spinnerets from µCT scans, same conventions as in Fig. 5. (**E**, **G**, **I-J**) Exemplary movement tracks of spinnerets active during the spinning of a silk anchorage, same conventions as in Fig. 5. (**F**, **H**) Light microscopy image of exemplary silk anchor on glass, same conventions as in Fig. 5.

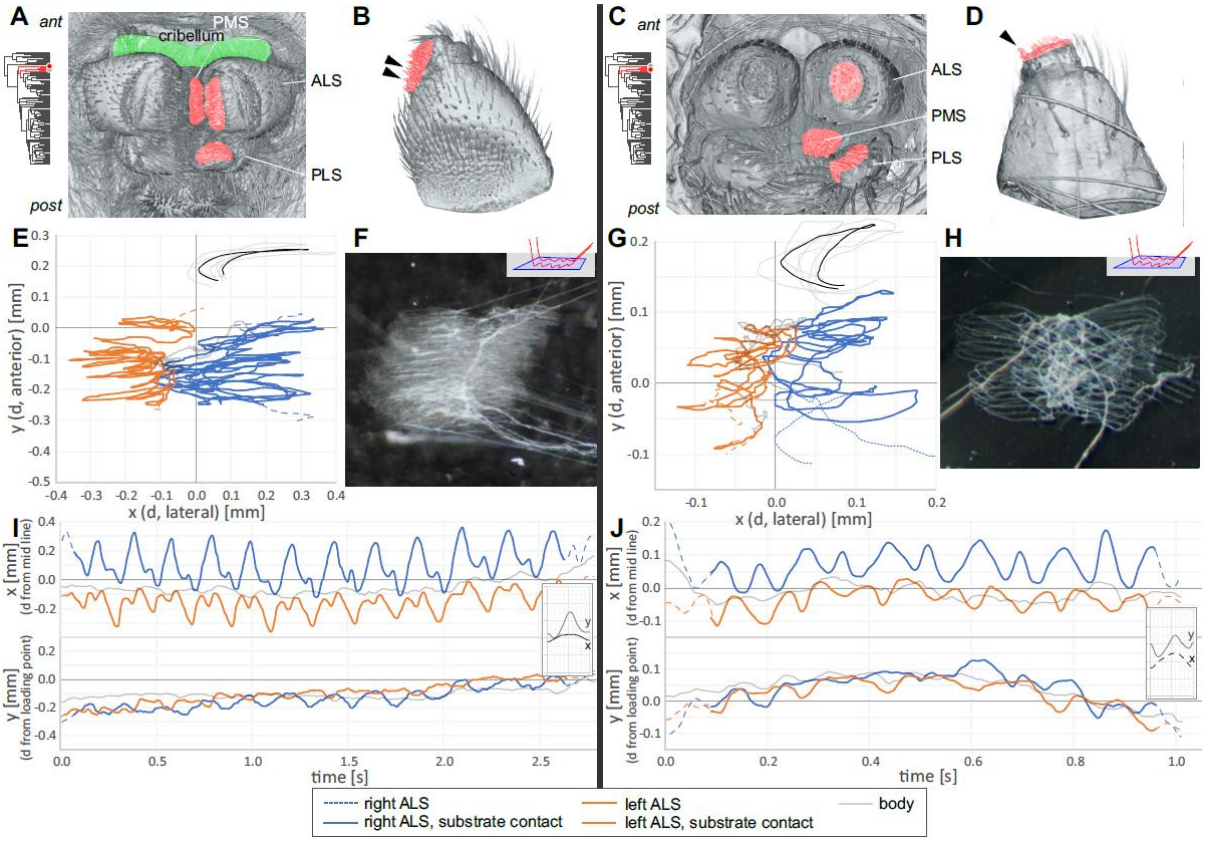

Fig. 12. Eresidae and Nicodamidae. (**A-B**, **E-F**, **I**) *Stegodyphus dumicola* (Eresidae), cribellar web builder. (**C-D**, **G-H**, **J**) *Oncodamus bidens* (Nicodamidae), ecribellar web builder. (**A-D**) 3D-reconstructions of spinnerets from µCT scans, same conventions as in Fig. 5. (**E**, **G**, **I-J**) Exemplary movement tracks of spinnerets active during the spinning of a silk anchorage, same conventions as in Fig. 5. (**F**, **H**) Light microscopy image of exemplary silk anchor on glass, same conventions as in Fig. 5.

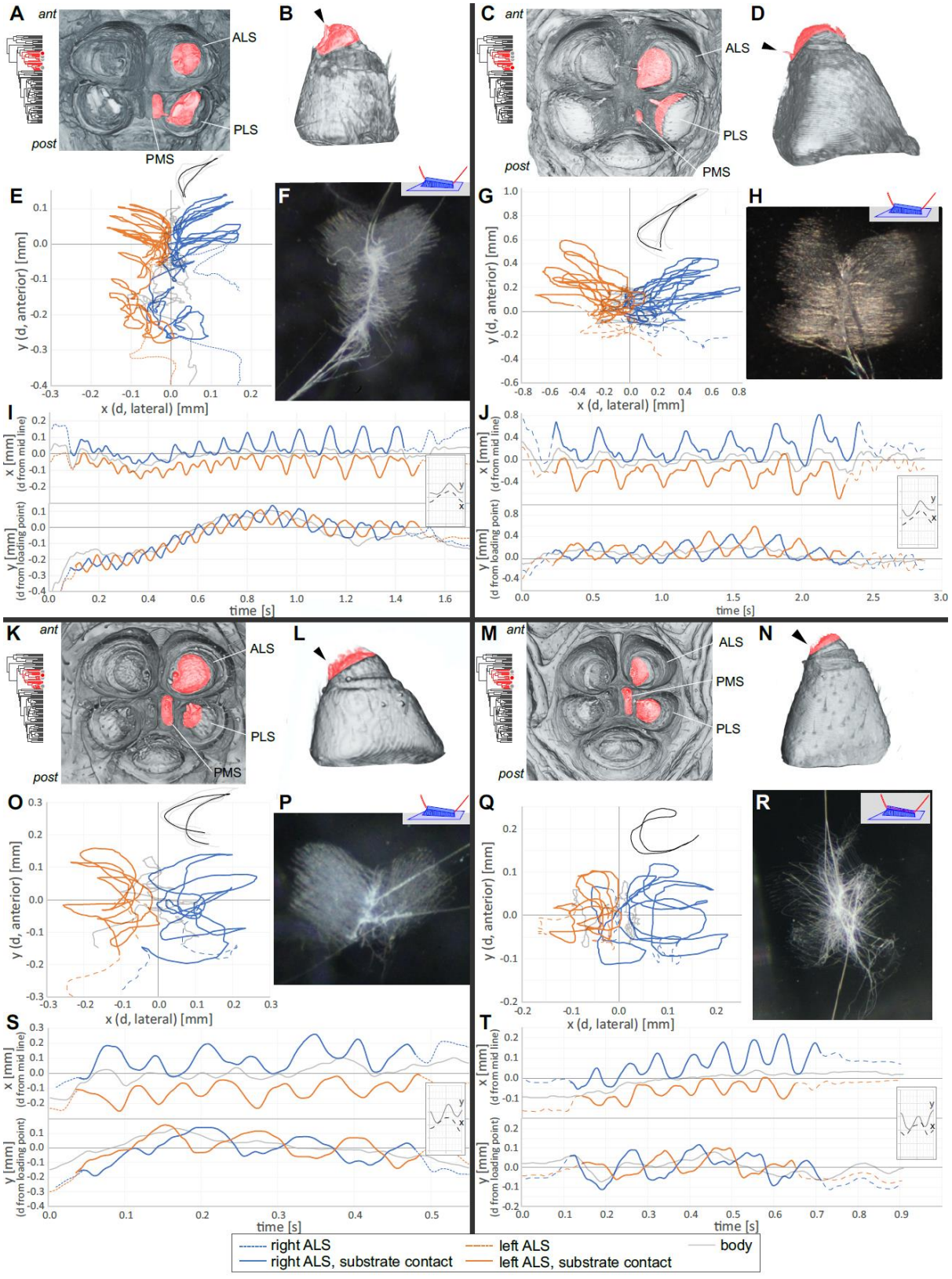

Fig. 13. Araneoidea. (**A-B**, **E-F**, **I**) *Cryptachaea gigantipes* (Theridiidae), ecribellar web builder. (**C-D**, **G-H**, **J**) *Argiope keyserlingi* (Araneidae), ecribellar web builder. (**K-L**, **O-P**, **S**) *Leucauge dromedaria* (Tetragnathidae), ecribellar web builder. (**M-N**, **Q-R**, **T**) *Arkys* spp., (Arkyidae), ecribellar hunting spiders, (**M-N**, **R**) *A. lancearius*, (**Q**, **T**) *A. furcatus*. (**A-D**, **K-N**) 3D-reconstructions of spinnerets from µCT scans, same conventions as in Fig. 5. (**E**, **G**, **I-J**, **O**, **Q**, **S-T**) Exemplary movement tracks of spinnerets active during the spinning of a silk anchorage, same conventions as in Fig. 5. (**F**, **H**, **P**, **R**) Light microscopy image of exemplary silk anchor on glass, same conventions as in Fig. 5.

Electronic Supplemental Material

S1. Material list with voucher information and sample sizes (pdf).

S2. Systematic description of anchor structure (pdf).

S3. Character matrix (csv).